Direct Observation of Sr Vacancies in $SrTiO_3$ by Quantitative Scanning Transmission Electron Microscopy

Honggyu Kim,* Jack Y. Zhang, Santosh Raghavan, and Susanne Stemmer†

Materials Department, University of California, Santa Barbara, California 93106-5050, USA

(Received 26 September 2016; revised manuscript received 14 November 2016; published 22 December 2016)

Unveiling the identity, spatial configuration, and microscopic structure of point defects is one of the key challenges in materials science. Here, we demonstrate that quantitative scanning transmission electron microscopy (STEM) can be used to directly observe Sr vacancies in $SrTiO_3$ and to determine the atom column relaxations around them. By combining recent advances in quantitative STEM, including variable-angle, high-angle annular dark-field imaging and rigid registration methods, with frozen phonon multislice image simulations, we identify which Sr columns contain vacancies and quantify the number of vacancies in them. Picometer precision measurements of the surrounding atom column positions show that the nearest-neighbor Ti atoms are displaced away from the Sr vacancies. The results open up a new methodology for studying the microscopic mechanisms by which point defects control materials properties.

DOI: 10.1103/PhysRevX.6.041063

Subject Areas: Condensed Matter Physics, Materials Science

I. INTRODUCTION

Recent advances in growth techniques for complex oxides have led to remarkable progress in the ability to control film stoichiometry, thereby enabling improvements in their properties, often by orders of magnitude [1]. Despite these successes, even small concentrations of unavoidable point defects can control the properties of complex oxides. In other cases, such defects are intentional, for example, for inducing superconductivity, metal-insulator transitions, and novel emergent phenomena [2–4]. $SrTiO_3$ is one of the most important complex oxides. The two prominent intrinsic point defects in $SrTiO_3$ are vacancies on the Sr and O sites, respectively. They play a key role in determining its properties. For example, Sr vacancies are a likely origin of ferroelectricity in $SrTiO_3$ [5,6], a material that is normally paraelectric at all temperatures. In doped $SrTiO_3$ films, Sr vacancies act as traps for carriers [7] and limit carrier mobilities [8]. Cation nonstoichiometry is thought to be responsible for the interface conductivity at the $LaAlO_3/SrTiO_3$ interface [9] and for resistive switching junctions with $SrTiO_3$ [10].

While methods to quantify the global concentration of point defects exist, determining their spatial arrangement, as well as direct information about atom relaxations around a point defect, is significantly more challenging, even though these are crucial for the properties. For example, lattice relaxations can determine whether or not a foreign atom acts as a dopant [11,12]. They can also be a signature of self-localization of charge carriers by interaction with the lattice (polaron formation) [13]. To date, this information has been obtained either indirectly (e.g., from vibrational spectroscopy) or from density functional theory (DFT). As a result, the precise microscopic structure of a point defect remains controversial in many cases.

High-angle annular dark-field (HAADF) imaging in scanning transmission electron microscopy (STEM) can image single impurity atoms that have a relatively large atomic number (Z) difference with the host crystal [14,15]. *Quantitative* HAADF-STEM [16] has been used to determine the three-dimensional dopant atom configurations with (near) unit-cell depth resolution [17,18]. Imaging of low-Z impurities or vacancies is substantially more challenging. The presence of vacancies has been inferred from STEM images in highly defective materials [19,20] and in materials in which vacancies form long-range ordered superlattice structures [21–23]. However, such studies have not yet provided quantitative, column-resolved information or the atomic arrangement around individual vacancies. More recently, it has been shown that variable-angle (VA) HAADF-STEM, which uses multiple detector configurations, improves contrast and interpretability [24]. Furthermore, image registration methods [25,26], applied to HAADF-STEM images acquired in series, allow for picometer precision measurements of atom column positions, a crucial capability for detecting small displacements around point defects.

As will be shown here, combining these advances opens the possibility of detecting not just foreign atoms with large Z contrast but also vacancies *and* their

*To whom all correspondence should be addressed.
kyuya380@gmail.com
†stemmer@mrl.ucsb.edu

associated local atom relaxations. We demonstrate direct imaging of Sr vacancies in $SrTiO_3$ and determine the lattice relaxation around the vacancies with picometer precision. We show that rigid registration methods not only improve the precision in measurements of atom column positions but also the quantification of image intensities, as needed to detect point defects with low Z contrast, such as vacancies. We show that the number of vacancies in each column can be quantified. Discrepancies between the measured lattice relaxations and predictions from DFT simulations underscore the need for atomic-scale experimental input in developing a microscopic understanding of how point defects control real materials properties.

II. EXPERIMENTAL

A 150-nm-thick, epitaxial $SrTiO_3$ film was grown on (001) $SrTiO_3$ using hybrid molecular beam epitaxy [27]. In this method, the film stoichiometry is controlled by the flux ratio of the metal-organic Ti source, Ti-tetraisopropoxide (TTIP), and elemental Sr, and is monitored using *in situ* reflection high-energy electron diffraction (RHEED) and x-ray diffraction, as described in detail elsewhere [8,28]. The $SrTiO_3$ film studied in this work was grown under slightly Sr-deficient conditions with a TTIP/Sr ratio of 60 (see Ref. [29] for an estimate of the Sr vacancy concentration). Plan-view transmission electron microscopy (TEM) samples were prepared using wedge polishing with a 1° angle. HAADF-STEM images were recorded using an FEI Titan S/TEM ($C_s = 1.2$ mm) operating at 300 keV with a convergence angle of 9.6 mrad. Two HAADF detector angular ranges, 60–390 and 47–306 mrad, were selected by choosing camera lengths of 100 and 130 cm, respectively. To improve the signal-to-noise ratio while avoiding scan distortions, 30 fast-scan images (1024×1024 pixels, 2 s frame time, 1.9 μs dwell time) were sequentially recorded from the same area and aligned post-acquisition using a cross-correlation algorithm.

The position of every atomic column in series-averaged HAADF images was determined by fitting to a two-dimensional (2D) Gaussian function. From the HAADF image, atomic column intensities for Sr and Ti-O columns (I_{Sr} and $I_{Ti\text{-}O}$) were measured by averaging intensities within a small disk, with a radius of one-fourth of a lattice constant of $SrTiO_3$, around each atomic column position. This method has been demonstrated to be a very effective way to obtain quantitative structural information since the integrated intensity is robust to subtle changes in imaging parameters such as defocus, effective source size, convergence angle, image noise, and sample tilt, all of which are difficult to determine experimentally [30,31].

Images of $SrTiO_3$ with different thicknesses were simulated using the Kirkland multislice algorithm [32] for both detector angular ranges with and without thermal diffuse scattering (TDS), as shown in Fig. S5 [29]. A 4×4 $SrTiO_3$ supercell was sampled with a 1024×1024 pixel grid. To create a supercell containing Sr vacancies, Sr atoms were removed from a single Sr atomic column of the ideal structure. Depending on the number of atoms and vacancies in a column, many different configurations are possible. A total number of 512 vacancy configurations were considered in this study: six and seven unit cells containing one to three vacancies, and eight and nine unit cells having between one and four vacancies. To reduce impractically long computation times, simulations for Sr-vacancy-containing $SrTiO_3$ were performed without TDS. As described in Ref. [17], the effect of TDS was then accounted for post-simulation by scaling the Sr and Ti-O intensities with scaling factors (I_{TDS} vs. $I_{no\text{-}TDS}$), determined from Fig. S5 [29].

It is important to determine a criterion for vacancy detection, i.e., to distinguish the signal induced by vacancies from experimental errors in HAADF imaging. For this purpose, quantitative HAADF-STEM was first performed on the $SrTiO_3$ substrate. As discussed in Ref. [17], the spread of the experimental data points around a linear fit can be modeled with a normal probability distribution, with the standard deviation used to approximate the error. This is described in detail in Fig. S1 of Ref. [29].

To estimate the number of Sr vacancies, the probabilities of the experimental data points corresponding to simulated configurations and thicknesses are calculated using the following equation:

$$p_i = \frac{\mathrm{norm}_i(t)}{\sum_n \mathrm{norm}_n(t)}, \tag{1}$$

where t is the distance between a simulated point and an experimental data point in I_{Sr} vs $I_{Ti\text{-}O}$ plots, normalized to the experimental error (S_X), and norm(t) is the standard normal distribution function:

$$\mathrm{norm}(t) = \frac{1}{\sqrt{2\pi}} e^{-(t^2/2)}. \tag{2}$$

The likely thicknesses of the column for an experimental data point were first determined based on $I_{Ti\text{-}O}$. As an independent thickness estimate, position-averaged convergent-beam electron diffraction (PACBED) [33] was also employed (Fig. S6, Ref. [29]). To calculate the probabilities of having a certain number of Sr vacancies in a column, we used the average distance from an experimental data point to each simulated configuration having a specific number of vacancies. For example, to calculate the probability of having one vacancy in six unit cells, the distances from an experimental data point to simulated points of all six possible configurations are averaged. For the combined detector, norm(t) values from each detector are multiplied for the probability calculations.

Electron beam damage may also induce a decrease in HAADF signal. To ensure that beam damage was negligible, the integrated intensities of columns A and B (see Fig. 1) from each frame (30 frames in total) during the serial image acquisition were extracted for both detectors (see Fig. S7, Ref. [29]). Throughout the sequential image acquisition with both detectors, signals from columns A and B remain unchanged without any abrupt intensity drop, indicating that there was no knock-on damage during the image acquisition.

III. RESULTS AND DISCUSSION

Figures 1(a) and 1(d) show series-averaged (rigid registration), quantitative HAADF images along ⟨001⟩ of a Sr-deficient $SrTiO_3$ film, recorded from the same region with the two different detector settings. Intensity maps of the Sr (I_{Sr}) and Ti-O ($I_{Ti\text{-}O}$) columns extracted from the images are shown in Figs. 1(b) and 1(c) and 1(e) and 1(f), respectively.

As described in the experimental section, an experimental error function for the column intensity measurements can be determined. This error limits the quantitative interpretation of the image intensity in terms of visibility, concentration, and depth configuration of a point defect(s) in a column under the given experimental condition. To detect Sr vacancies, Sr columns with intensity values that fall outside the experimental error are identified. Series-averaged images substantially reduce the error compared to a single acquisition. This is particularly true for detector 1, where the error was reduced by 70% (see Ref. [29]). Thus, (rigid) registration is not only beneficial for determining atom column positions (see Refs. [25,26]), but it also improves interpretability of the image contrast, which is key to detecting vacancies.

Two Sr columns, labeled A and B in Figs. 1(a) and 1(d), have intensities that lie below the lower bound of the error cutoff function for both detectors (dotted line in Fig. S1 [29]). The four Ti-O columns ($I_{Ti\text{-}O}$) surrounding columns A and B serve as a measure of the local thickness [17]. While I_{Sr} of columns A and B are much lower than the neighboring Sr columns [see arrows in Figs. 1(b) and 1(e)], the intensities ($I_{Ti\text{-}O}$) of their four surrounding Ti-O columns are relatively uniform [see white boxes in Figs. 1(c) and 1(f)]. Thus, the distinctly lower I_{Sr} of columns A and B is not the result of thickness variations. Instead, the most plausible source for the low intensities in these columns is Sr vacancies.

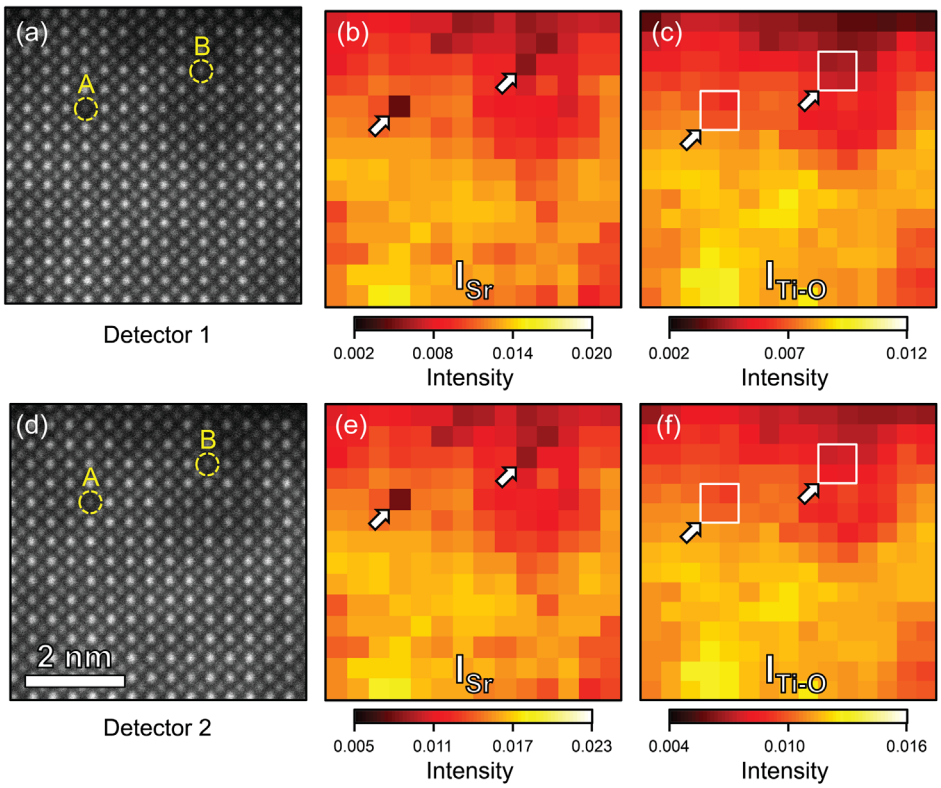

FIG. 1. Quantitative, rigidly registered, variable-angle HAADF-STEM images of Sr vacancies in a $SrTiO_3$ film grown by MBE. (a,d) HAADF STEM images of the $SrTiO_3$ film recorded with detectors 1 and 2, respectively. Image intensities are normalized to the incident beam intensity (see scale bars). I_{Sr} and $I_{Ti\text{-}O}$ maps are displayed in (b,e) and (c,f), respectively. The Sr columns containing Sr vacancies are labeled A and B and indicated by white arrows in (b) and (e). The four nearest-neighboring Ti-O columns for columns A and B are marked by white boxes in (c) and (f), showing relatively uniform image contrast.

To estimate the number of vacancies in these columns, we performed frozen phonon simulations for all possible configurations of 1–3 Sr vacancies for sample thickness of 6 and 7 unit cells (UCS) and 1–4 Sr vacancies for sample thicknesses of 8 and 9 UCS. The calculated I_{Sr} vs $I_{Ti\text{-}O}$ for all of these configurations for both detectors are shown in Fig. 2 along with the experimental data (squares). Each orange circle in Fig. 2 corresponds to a specific vacancy configuration for a given foil thickness, i.e., a single vacancy in all possible depth positions, two vacancies in all possible configurations, etc. To determine the most likely number of Sr vacancies in column A, the experimental I_{Sr} (red square) was compared with those for all possible defect configurations for 8 and 9 UC thickness, as the experimental $I_{Ti\text{-}O}$ falls in between these two thicknesses. In the same manner, the intensity of column B (green square) was compared with the calculated intensities for 6 and 7 UCS. The probabilities for each configuration were calculated for each detector and then combined, taking into account the experimental error function [17,24,29]. The results are listed in Table I. As can be seen, one can conclude with very high confidence that column A contains three vacancies in a 8-UC thick sample and that column B contains two vacancies in a 7-UC thick sample (both therefore contain 5 Sr atoms). The advantage of using two detectors can be clearly seen: The probability of determining the correct number is significantly improved using the combined information from two independent experiments with different detector settings. The approach is particularly beneficial for column B, where the probability of identifying the correct position is only 43% with detector 1 but increases to 93% by using both detectors. Although the number of vacancies can be determined, the I_{Sr} of the possible configurations for a given number of vacancies are too similar to determine the positions of the vacancies within the column with unit cell resolution (see Fig. S2 in Ref. [29]).

In principle, Sr deficiency could also be accommodated by Ti antisite defects or Ti interstitials. Because of space constraints in the perovskite unit cell, Ti interstitials have high formation energies compared to Sr vacancies and are thus unlikely to form [34,35]. Ti antisite defects would

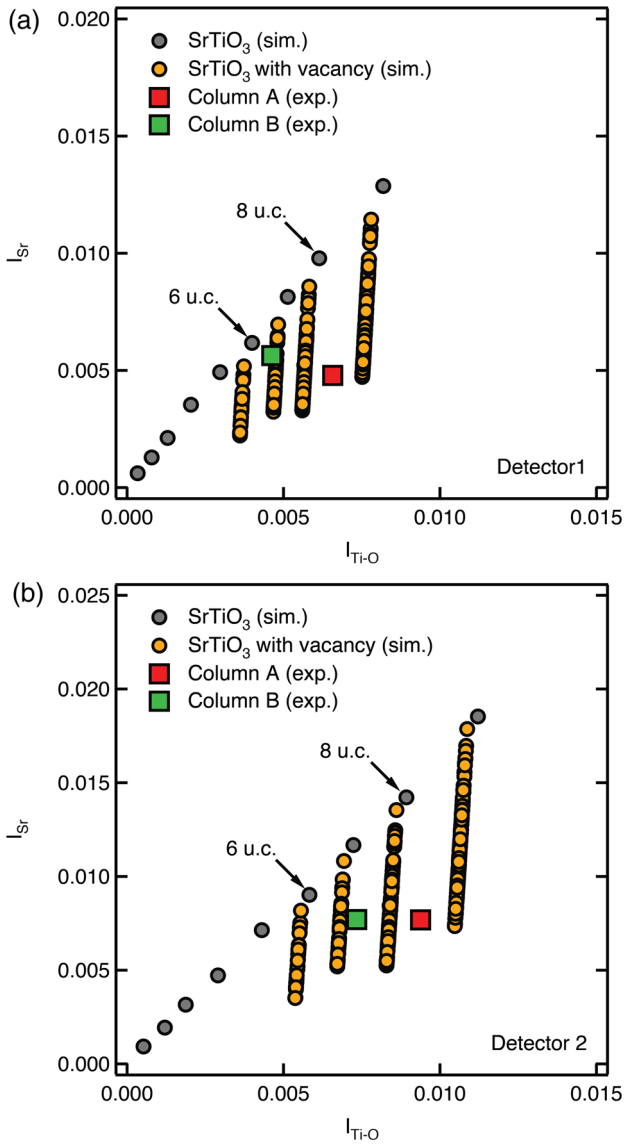

FIG. 2. Determination of vacancy configurations. (a,b) Simulated I_{Sr} vs $I_{Ti\text{-}O}$ plots using detector angular ranges corresponding to detectors 1 and 2. Red and green squares represent the intensities from columns A and B, respectively, while orange circles are the simulated data points for all possible vacancy configurations.

TABLE I. Probability of Sr vacancy configurations. Probabilities of determining the correct number of Sr vacancies in column A and B using the different detector information: detector 1; detector 2; combined detector. Configurations with probabilities of less than 0.01% are not listed.

Column A					Column B				
Thickness (UCS)	Number of vacancies	Probability (%)			Thickness (UCS)	Number of vacancies	Probability (%)		
		Detector 1	Detector 2	Combined			Detector 1	Detector 2	Combined
8	2	0.78	1.17	0.02	6	0	27.52	5.06	4.11
8	3	71.19	68.16	92.60	6	1	4.06	7.02	0.84
8	4	8.71	19.37	3.22	7	1	24.95	3.29	2.43
9	4	19.32	11.29	4.16	7	2	43.39	72.29	92.59
					7	3	0.08	12.01	0.03

also reduce I_{Sr}. However, I_{Sr} of column A is lower than that of its neighboring $I_{Ti\text{-}O}$ for both detectors. Thus, to invoke antisite defects, all Sr atoms in column A would have to be replaced by Ti atoms, along with vacancies. Such an extended defect would be energetically unfavorable and also visible in strain-contrast imaging [36], which is not consistent with our observations. At very large concentration of Ti excess (Sr deficiency), amorphous TiO_x phases [37] and/or Sr vacancy clusters [20] can form. These are relatively easy to detect in TEM but were not observed here.

Figures 3(b) and 3(d) show maps of the column distances around column A for each detector, measured from series-averaged HAADF images in Figs. 3(a) and 3(c), respectively. Each pixel represents the averaged distance from one cation column (i.e., Sr or Ti-O) to the four nearest-neighbor columns (i.e., Ti-O or Sr), as illustrated in Fig. 3(a). Both detectors clearly show lattice relaxations around column A, which contains the Sr vacancies. Specifically, atoms in the four nearest Ti-containing columns are displaced away from column A. Also note that the displacements are clearly associated with the column that showed the large decrease in I_{Sr}. The averaged distances are 2.88 and 2.85 Å for detectors 1 and 2, respectively, while for ideal $SrTiO_3$ it should be 2.76 Å. The precision in distance measurements is 1.5 pm, as determined from the standard deviation of atomic distances measured using the series-averaged HAADF image of the $SrTiO_3$ substrate (see Fig. S3 [29]). The displacement (about 10 pm) around the columns containing vacancies is significantly larger than this measurement uncertainty. Analysis of the columns around B gives a similar result of surrounding Ti atoms moving away from the column containing the Sr vacancies (Fig. S4 [29]). The actual displacement of the atoms in immediate proximity to the vacancies could be slightly larger as HAADF images are a projection and the measured displacements are thus an average. If there is a thickness dependence in the relaxations, the small differences between the two detectors may indeed be real (they are slightly larger than the error determined from Fig. S3 [29]). In particular, detector 1 (larger angles) is expected to be more sensitive to displacements further down the column (away from the entrance surface) because of the focusing action of the columns [24,38].

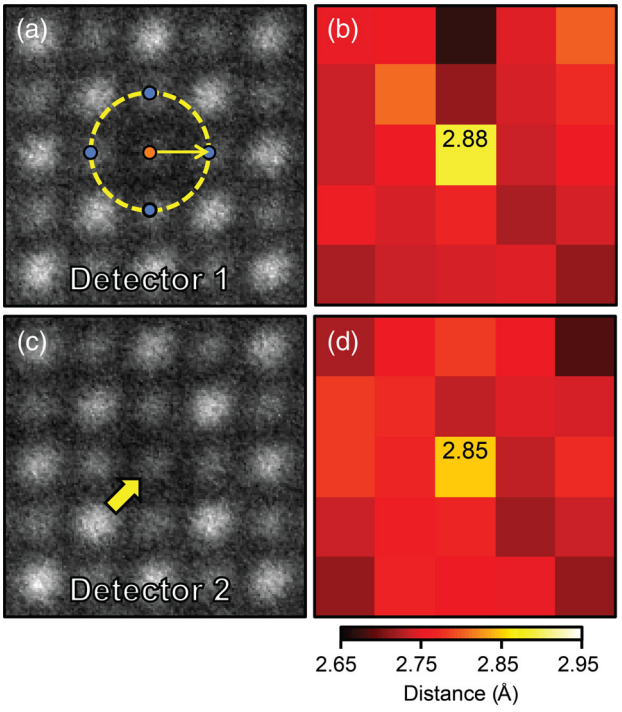

FIG. 3. Local structure relaxation around Sr vacancies. (a,c) Magnified HAADF STEM images near column-A recorded with detectors 1 and 2, respectively. (b,d) Atomic distance maps, where each pixel value indicates the average distance from one cation to its four nearest-neighbor unlike cations, showing Ti-O columns being displaced away from Sr vacancies. The overlay in (a) shows an example of a distance measurement from a Sr column (orange circle) to the Ti-O columns (blue circle).

The displacement of columns away from the Sr vacancies is consistent with the large lattice parameter expansion that has been measured in x-ray diffraction of Sr-deficient films [28,39,40]. The results are, however, in contradiction with theoretical studies reported in the literature. Such studies, which were carried out by several different methods (e.g., DFT local density approximation, DFT screened hybrid functionals, shell models, etc.), predict that only the nearest-neighbor *oxygen* atoms move away from the Sr vacancy, while the second-nearest-neighbor Ti atoms move *toward* the vacancy, resulting in a negligible overall lattice expansion, independent of the charge state of the vacancy [41,42,43]. Several possible reasons may exist for the discrepancies between DFT and experiment. The columns studied here contain more than one Sr vacancy, whereas DFT studies are for a single vacancy. However, our result appears to be independent of the number of vacancies: Both columns A and B give the same result, although the number of Sr vacancies in them is different. Although less likely, we cannot exclude that Sr vacancies form a more complex defect with oxygen vacancies, which cannot be detected in these experiments and has not yet been simulated in DFT. It would be interesting to conduct DFT simulations for this situation. Finally, there is also the possibility of systematic issues with the DFT calculations. For example, it has been shown that because DFT does not properly account for electron correlation effects, incorrect descriptions of energy levels, charge states, and atom relaxations are obtained for oxygen vacancies in $SrTiO_3$ [44]. It has also been reported that different DFT methods produce opposite results for the atom displacements around the oxygen vacancy in $SrTiO_3$ [45]. Most importantly, the discrepancy uncovered here shows that DFT alone may not capture the atomic structure of point defects in real materials—experimental input (and development of experimental techniques such as STEM) is clearly needed for accurate predictions of electronic

structure and properties, which depend on these structural relaxations. This conclusion is independent of the reason for the discrepancy, i.e., whether it is associated with the complexity of the defects in the real material or possible shortcomings of DFT.

IV. CONCLUSIONS

In summary, we have shown that Sr vacancies in $SrTiO_3$ can be directly observed in quantitative VA HAADF-STEM. The number of vacancies in each column can be determined with a high degree of confidence (>90%). An outward (away from the column containing Sr vacancies) displacement of Ti-O columns by about 10 pm was measured. These results allow for further developing electronic structure theory of these defects and for developing a microscopic understanding of how Sr vacancies control functional properties such as ferroelectricity and electrical transport. Future studies should be aimed at resolving the origin of the differences between experiment and DFT uncovered here, as the underlying reasons have implications beyond $SrTiO_3$.

More generally, the methodology described here is not limited to $SrTiO_3$ and hopefully will stimulate experimental and theoretical studies aiming at a microscopic understanding of the properties of point defects in other complex oxides and materials, which so far has been achieved for very few point defects (i.e., DX centers in III–V semiconductors). Finally, the results also point to further advances in quantitative STEM. In particular, quantitative, high-precision measurements of atom column displacements may allow for detection of point defects that do not affect image intensities within the detection limit. Moreover, the analysis of displacements using more than one detector may allow for depth-resolved information of the displacements. While this was not possible in the present experiments because of the presence of multiple vacancies in the columns, which reduces any depth dependence of the displacements, size-mismatched dopant atoms with a relative large Z contrast may be an ideal test case to develop this capability. It would allow a complete, three-dimensional characterization of point defects not possible by *any* other method.

ACKNOWLEDGEMENTS

This work was supported by the U.S. Department of Energy (Grant No. DEFG02-02ER45994). Film growth experiments were supported by the Materials Research Science and Engineering Centers Program of the National Science Foundation under Grant No. DMR 1121053, which also supported the Shared Experimental Facilities used in this work. H. K. and S. S. gratefully acknowledge the Center for Scientific Computing at the California Nanosystems Institute and the support from the National Science Foundation (Grant No. CNS-0960316).

[1] D. G. Schlom, *Perspective: Oxide Molecular-Beam Epitaxy Rocks!*, APL Mater. **3**, 062403 (2015).
[2] P. A. Lee, N. Nagaosa, and X.-G. Wen, *Doping a Mott Insulator: Physics of High-Temperature Superconductivity*, Rev. Mod. Phys. **78**, 17 (2006).
[3] E. Miranda and V. Dobrosavljevic, *Disorder-Driven Non-Fermi Liquid Behaviour of Correlated Electrons*, Rep. Prog. Phys. **68**, 2337 (2005).
[4] E. Abrahams and G. Kotliar, *The Metal-Insulator Transition in Correlated Disordered Systems*, Science **274**, 1853 (1996).
[5] H. W. Jang *et al.*, *Ferroelectricity in Strain-Free* $SrTiO_3$ *Thin Films*, Phys. Rev. Lett. **104**, 197601 (2010).
[6] D. Lee *et al.*, *Emergence of Room-Temperature Ferroelectricity at Reduced Dimensions*, Science **349**, 1314 (2015).
[7] Y. Kozuka, Y. Hikita, C. Bell, and H. Y. Hwang, *Dramatic Mobility Enhancements in Doped* $SrTiO_3$ *Thin Films by Defect Management*, Appl. Phys. Lett. **97**, 012107 (2010).
[8] A. P. Kajdos and S. Stemmer, *Surface Reconstructions in Molecular Beam Epitaxy of* $SrTiO_3$, Appl. Phys. Lett. **105**, 191901 (2014).
[9] M. P. Warusawithana *et al.*, $LaAlO_3$ *Stoichiometry Is Key to Electron Liquid Formation at* $LaAlO_3/SrTiO_3$ *Interfaces*, Nat. Commun. **4**, 2351 (2013).
[10] E. Mikheev, J. Hwang, A. P. Kajdos, A. J. Hauser, and S. Stemmer, *Tailoring Resistive Switching in* $Pt/SrTiO_3$ *Junctions by Stoichiometry Control*, Sci. Rep. **5**, 11079 (2015).
[11] P. M. Mooney, *Deep Donor Levels (DX Centers) in III-V Semiconductors*, J. Appl. Phys. **67**, R1 (1990).
[12] H. J. Queisser and E. E. Haller, *Defects in Semiconductors: Some Fatal, Some Vital*, Science **281**, 945 (1998).
[13] D. Emin, *Polarons* (Cambridge University Press, Cambridge, 2013).
[14] P. M. Voyles, D. A. Muller, J. L. Grazul, P. H. Citrin, and H. J. L. Gossmann, *Atomic-Scale Imaging of Individual Dopant Atoms and Clusters in Highly n-Type Bulk Si*, Nature (London) **416**, 826 (2002).
[15] S. H. Oh, K. van Benthem, S. I. Molina, A. Y. Borisevich, W. D. Luo, P. Werner, N. D. Zakharov, D. Kurnar, S. T. Pantelides, and S. J. Pennycook, *Point Defect Configurations of Supersaturated Au Atoms inside Si Nanowires*, Nano Lett. **8**, 1016 (2008).
[16] J. M. LeBeau, S. D. Findlay, L. J. Allen, and S. Stemmer, *Quantitative Atomic Resolution Scanning Transmission Electron Microscopy*, Phys. Rev. Lett. **100**, 206101 (2008).
[17] J. Hwang, J. Y. Zhang, A. J. D'Alfonso, L. J. Allen, and S. Stemmer, *Three-Dimensional Imaging of Individual Dopant Atoms in* $SrTiO_3$, Phys. Rev. Lett. **111**, 266101 (2013).
[18] R. Ishikawa, A. R. Lupini, S. D. Findlay, T. Taniguchi, and S. J. Pennycook, *Three-Dimensional Location of a Single Dopant with Atomic Precision by Aberration-Corrected Scanning Transmission Electron Microscopy*, Nano Lett. **14**, 1903 (2014).
[19] D. A. Muller, N. Nakagawa, A. Ohtomo, J. L. Grazul, and H. Y. Hwang, *Atomic-Scale Imaging of Nanoengineered Oxygen Vacancy Profiles in* $SrTiO_3$, Nature (London) **430**, 657 (2004).
[20] Y. Tokuda, S. Kobayashi, T. Ohnishi, T. Mizoguchi, N. Shibata, Y. Ikuhara, and T. Yamamoto, *Strontium Vacancy Clustering in Ti-Excess* $SrTiO_3$ *Thin Film*, Appl. Phys. Lett. **99**, 033110 (2011).

[21] N. Biskup, J. Salafranca, V. Mehta, M. P. Oxley, Y. Suzuki, S. J. Pennycook, S. T. Pantelides, and M. Varela, *Insulating Ferromagnetic* $LaCoO_{3-\partial}$ *Films: A Phase Induced by Ordering of Oxygen Vacancies*, Phys. Rev. Lett. **112**, 087202 (2014).

[22] Y. M. Kim, J. He, M. D. Biegalski, H. Ambaye, V. Lauter, H. M. Christen, S. T. Pantelides, S. J. Pennycook, S. V. Kalinin, and A. Y. Borisevich, *Probing Oxygen Vacancy Concentration and Homogeneity in Solid-Oxide Fuel-Cell Cathode Materials on the Subunit-Cell Level*, Nat. Mater. **11**, 888 (2012).

[23] D. O. Klenov, W. Donner, B. Foran, and S. Stemmer, *Impact of Stress on Oxygen Vacancy Ordering in Epitaxial* $(La_{0.5}Sr_{0.5})CoO_{3-\partial}$ *Thin Films*, Appl. Phys. Lett. **82**, 3427 (2003).

[24] J. Y. Zhang, J. Hwang, B. J. Isaac, and S. Stemmer, *Variable-Angle High-Angle Annular Dark-Field Imaging: Application to Three-Dimensional Dopant Atom Profiling*, Sci. Rep. **5**, 12419 (2015).

[25] A. B. Yankovich, B. Berkels, W. Dahmen, P. Binev, S. I. Sanchez, S. A. Bradley, A. Li, I. Szlufarska, and P. M. Voyles, *Picometre-Precision Analysis of Scanning Transmission Electron Microscopy Images of Platinum Nanocatalysts*, Nat. Commun. **5**, 4155 (2014).

[26] X. H. Sang and J. M. LeBeau, *Revolving Scanning Transmission Electron Microscopy: Correcting Sample Drift Distortion without Prior Knowledge*, Ultramicroscopy **138**, 28 (2014).

[27] B. Jalan, R. Engel-Herbert, N. J. Wright, and S. Stemmer, *Growth of High-Quality* $SrTiO_3$ *Films Using a Hybrid Molecular Beam Epitaxy Approach*, J. Vac. Sci. Technol. A **27**, 461 (2009).

[28] B. Jalan, P. Moetakef, and S. Stemmer, *Molecular Beam Epitaxy of* $SrTiO_3$ *with a Growth Window*, Appl. Phys. Lett. **95**, 032906 (2009).

[29] See Supplemental Material at http://link.aps.org/supplemental/10.1103/PhysRevX.6.041063 for experimental and simulated I_{Sr} vs $I_{Ti\text{-}O}$ for the $SrTiO_3$ substrate as a function of thicknesses, estimates of the Sr vacancy concentration, series-averaged HAADF of the $SrTiO_3$ substrate, simulated images of vacancy configurations and results for their positions, atom column displacements around column B, simulations with and without TDS for $SrTiO_3$, PACBED pattern, and intensities measured for the individual frames.

[30] K. E. MacArthur, A. J. D'Alfonso, D. Ozkaya, L. J. Allen, and P. D. Nellist, *Optimal ADF STEM Imaging Parameters for Tilt-Robust Image Quantification*, Ultramicroscopy **156**, 1 (2015).

[31] H. E, K. E. MacArthur, T. J. Pennycook, E. Okunishi, A. J. D'Alfonso, N. R. Lugg, L. J. Allen, and P. D. Nellist, *Probe Integrated Scattering Cross Sections in the Analysis of Atomic Resolution HAADF STEM Images*, Ultramicroscopy **133**, 109 (2013).

[32] E. J. Kirkland, *Advanced Computing in Electron Microscopy* (Springer, New York, 2010).

[33] J. M. LeBeau, S. D. Findlay, L. J. Allen, and S. Stemmer, *Position Averaged Convergent Beam Electron Diffraction: Theory and Applications*, Ultramicroscopy **110**, 118 (2010).

[34] M. J. Akhtar, Z. U. N. Akhtar, R. A. Jackson, and C. R. A. Catlow, *Computer Simulation Studies of Strontium Titanate*, J. Am. Ceram. Soc. **78**, 421 (1995).

[35] N. H. Chan, R. K. Sharma, and D. M. Smyth, *Nonstoichiometry in* $SrTiO_3$, J. Electrochem. Soc. **128**, 1762 (1981).

[36] M. Choi, F. Oba, and I. Tanaka, *Role of Ti Antisitelike Defects in* $SrTiO_3$, Phys. Rev. Lett. **103**, 185502 (2009).

[37] T. Suzuki, Y. Nishi, and M. Fujimoto, *Defect Structure in Homoepitaxial Non-stoichiometric Strontium Titanate Thin Films*, Phil. Mag A **80**, 621 (2000).

[38] A. Mittal and K. A. Mkhoyan, *Limits in Detecting an Individual Dopant Atom Embedded in a Crystal*, Ultramicroscopy **111**, 1101 (2011).

[39] T. Ohnishi, K. Shibuya, T. Yamamoto, and M. Lippmaa, *Defects and Transport in Complex Oxide Thin Films*, J. Appl. Phys. **103**, 103703 (2008).

[40] C. M. Brooks, L. F. Kourkoutis, T. Heeg, J. Schubert, D. A. Muller, and D. G. Schlom, *Growth of Homoepitaxial* $SrTiO_3$ *Thin Films by Molecular-Beam Epitaxy*, Appl. Phys. Lett. **94**, 162905 (2009).

[41] T. Tanaka, K. Matsunaga, Y. Ikuhara, and T. Yamamoto, *First-Principles Study on Structures and Energetics of Intrinsic Vacancies in* $SrTiO_3$, Phys. Rev. B **68**, 205213 (2003).

[42] A. Janotti, J. B. Varley, M. Choi, and C. G. van de Walle, *Vacancies and Small Polarons in* $SrTiO_3$, Phys. Rev. B **90**, 085202 (2014).

[43] D. A. Freedman, D. Roundy, and T. A. Arias, *Elastic Effects of Vacancies in Strontium Titanate: Short- and Long-Range Strain Fields, Elastic Dipole Tensors, and Chemical Strain*, Phys. Rev. B **80**, 064108 (2009).

[44] C. W. Lin and A. A. Demkov, *Electron Correlation in Oxygen Vacancy in* $SrTiO_3$, Phys. Rev. Lett. **111**, 217601 (2013).

[45] C. Mitra, C. Lin, J. Robertson, and A. A. Demkov, *Electronic Structure of Oxygen Vacancies in* $SrTiO_3$ *and* $LaAlO_3$, Phys. Rev. B **86**, 155105 (2012).